Check for updates

ChemistrySelect

Research Article
doi.org/10.1002/slct.202404728

Chemistry Europe
European Chemical Societies Publishing

www.chemistryselect.org

Development of Vincristine-Loaded Nano Graphene Oxides for Dual Therapies Against Canine Anaplastic Carcinoma Cells Obtained From a Dog with Spontaneous Mammary Tumor

Yunus Emre Atay,[a] Sadi Yusufbeyoğlu,[b] Zuhal Hamurcu,[c] Ahsen Güler,[c] Latife Çakir Bayram,[d] Görkem Ekebaş,[d] Cagla Celik,[e] Cemile Yilmaz,[f] Ismail Ocsoy,*[f] and Yaşar Akar*[a]

Among pet species, mammary tumors are most commonly encountered in dogs. In the traditional treatment of mammary tumors in dogs; surgical operation, chemotherapy, immunotherapy, cryotherapy, radiotherapy and homeopathy are used. Herein, we reported vincristine loaded nano graphene oxide (Vin@nGO) for simultaneous photothermal therapy (PTT) and chemotherapy under near infrared laser (NIR, 808 nm), whereas GO was used both as a platform for vincristine and as a photothermal (PT) agent, and vincristine was used as a chemotherapeutic agent. Spontaneous mammary tumor masses of a dog were removed and primary tumor cells were obtained and propagated by tissue culture from tumor tissue samples under appropriate conditions. Then, these cells were incubated with Vin@nGO and exposed to NIR laser. NIR laser irradiation at 808 nm was converted to heat by nGO, then the target cancer cells were destroyed by both hyperthermia and chemotherapy. MTS analysis was performed to test the effectiveness of this dual therapy on cell proliferation and a statistically significant ($p < 0.05$) decrease in cell proliferation/viability was found (90% reduction compared to the control group ($p < 0.0001$)). Our study data also shed light on usability of Vin@nGO in the in *vivo* model for future work.

1. Introduction

Among domestic animal species, mammary tumors are most common in dogs,[1,2] and in recent years, mammary tumors have been among the most important causes of death in pets.[3] The 50% of all tumors seen in female dogs is mammary tumors.[1] Mammary tumors in dogs are consisting of luminal epithelial cells, mesenchymal cells, myoepithelial cells or interstitial connective tissues.[4,5,6] The advanced age, nutrition, environmental factors, some steroid hormones, cycle disorders, immunological, and genetic predisposition can be considered as potential factors for the formation and progression of mammary tumors in dogs and cats.[1,7] Although conventional treatment models performed for mammary tumors in dogs are surgical operation, chemotherapy, radiotherapy, immunotherapy, hormonal treatment, homeopathy, cryotherapy, and phototherapy; the gold standard treatment for canine mammary tumors in veterinary clinics is surgical removal of the mass.[1,3,7–9]

Today, although chemotherapy is one of the most important treatment options, however, its use is limited due to the resistance of cancer cells, the severe harmful side effects of anticancer drugs on normal tissues and organs, and the risks of metastasis and recurrence.[3] Photothermal therapy (PTT) known as a noninvasive therapy relies on conversion of absorbed NIR laser irradiation by the special nanomaterials (NMs) into heat, which causes increase in temperature of the reaction environment (range of 42 °C and 47 °C) and induces cell death.[10–20] The reported study shows that after gold nanorod (Au NR) based PTT application, complete and partial remission of the tumors were observed in 62.5% and 25% of treated animals (dogs and cats) respectively. In addition to that no tumor growth was seen 12.5% of treated animals.[3] We interpret that this promising results indicate effectiveness of the PTT toward solid tumor. However, the major drawback of Au NR is toxicity of ligand (cetyltrimethylammonium bromide).

In this study, we reported vincristine loaded nano graphene oxide (Vin@nGO) with PTT and chemotherapy toward canine mammary tumor cells obtained from tumoral masses of a dog with spontaneous mammary tumors. These masses were surgically removed under general anesthesia, and then used for

[a] *Dr. Y. E. Atay, Y. Akar*
Department of Obstetrics and Gyneacology, Faculty of Veterinary Medicine, Erciyes University, Kayseri 38280, Türkiye
E-mail: yasarakar@erciyes.edu.tr

[b] *Prof. Dr. S. Yusufbeyoğlu*
Department of Pharmaceutical Botany, Faculty of Gulhane Pharmacy, University of Health Sciences, Ankara 06018, Türkiye

[c] *Prof. Dr. Z. Hamurcu, A. Güler*
Department of Medical Biology, Faculty of Medicine, Betül-Ziya Eren Genome and Stem Cell Center, Erciyes University, Kayseri 38280, Türkiye

[d] *Prof. Dr. L. Ç. Bayram, Dr. G. Ekebaş*
Department of Pathology, Faculty of Veterinary Medicine, Erciyes University, Kayseri 38280, Türkiye

[e] *Dr. C. Celik*
Department of Analytical Chemistry, Faculty of Pharmacy, Harran University, Şanlıurfa 63000, Türkiye

[f] *C. Yilmaz, Prof. Dr. I. Ocsoy*
Department of Analytical Chemistry, Faculty of Pharmacy, Erciyes University, Kayseri 38280, Türkiye
E-mail: ismailocsoy@erciyes.edu.tr

© 2024 Wiley-VCH GmbH

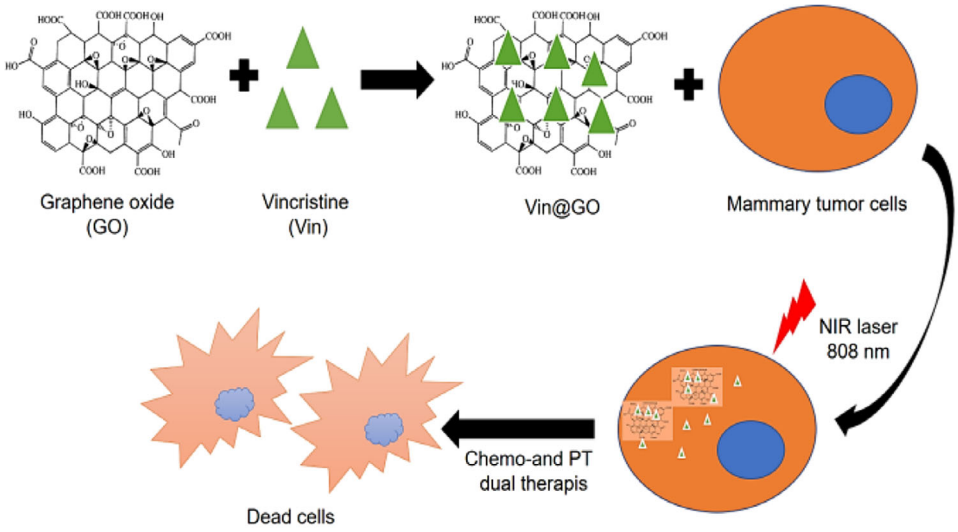


Figure 1. Illustration of synthesis Vin@nGO and cancer cell death via dual therapies.

histopathological evaluation and for primary cell culture in appropriate media (tissue culture). These cells are then divided into different groups: (i) control cell line (without any treatment), (ii) NIR laser irradiation, (iii) vincristine, (iv) vincristine + NIR laser irradiation, (v) GO, (vi) GO + NIR laser irradiation, (vii) Vin@nGO and (viii) Vin@nGO + NIR laser irradiation. The functions of the GO are a platform of vincristine conjugation and a PTT agent for conversion of NIR light into heat. After discovery of graphene in 2004, GO was produced from graphene as its the oxidized form and has been actively used in various scientific and industrial fields owing to its great physical, chemical, mechanical, and electronic properties.[21–30] It is also used for biomedical applications with its water-solubility, hydrophobic/hydrophilic drug loading capability and controlled release efficiency,[27–30] whereas vincristine (vin) is kind of a first drug to treat canine transmissible venereal tumor.[31] It is also one of the most commonly used chemotherapeutic drugs for canine mammary tumors.[9,32–35] Although vincristine has still been actively used in clinics, it can adversely affect bone marrow or the gastro intestinal system and it may result in new resistance.[36] Vincristine has been actively used in various cancer types for scientific and clinical research. Additionally, vincristine can be seen as an effective candidate for treatment of some other haematological diseases like thrombocytopenic purpura and chronic idiopathic thrombocytopenia. It also is suitable for combination therapy with various commonly used drugs in the management of various cancer disease.[37,38]

2. Results and Discussion

We prepared Vin@nGO for simultaneous and dual PTT and chemotherapy under near infrared laser (NIR, 808 nm). Vincristine was immobilized on the surface of GO via π-π stacking interactions. In Figure 1, we demonstrated preparation of Vin@nGO, incubation with target cancer cells and their destruction via chemotherapy and PTT under NIR laser irradiation.

2.1. Histopathological Findings

As shown in Figure 2 that the case was anaplastic carcinoma (malignant carcinoma) based upon histopathological and immunohistochemical examination. Neoplastic proliferation of anaplastic epithelial cells was accompanied by abundant fibrovascular stroma. Marked cellular atypia demonstrated by marked anisocytosis and karyomegaly was observed. A tumor was present consisting of a proliferation of highly pleomorphic epithelial cells, unrestricted and unencapsulated, organized as individual groups and forming papillary projections interspersed with prominent fibrovascular stroma. These cells showed several features of malignancy, including marked anisocytosis and anisokaryosis, karyomegaly, and coarse chromatin. Widespread invasion of lymphatic vessels was noted.

The primary tumor corresponded to a round mass of epithelial cells arranged in sheets separated by wide trabeculae of connective tissue, displaying a strong vascular invasion by neoplastic cells. Extensive necrotic areas were visible. Neoplastic cells were frequently individualized or arranged in small nest often surrounded by collagen fibers (desmoplasia). Small and rare areas of tubular differentiation can be identified. The predominant tumor cells are round or deformed due to close contact. The cytoplasm is acidophilic, and the large nucleus is very often deformed, hyperchromatic, with the nucleolus rarely identified. Epithelial cells generally formed tubular and solid structures (one case), whereas atypical spindle cell proliferations were intensely observed in the stroma and intertubular areas. In addition to spindle-shaped cells in the intertubular areas, the presence of large, polygonal cells with transparent cytoplasm was remarkable. Anisocytosis, hyperchromasia and hypochromasia were quite prominent in the luminal epithelial cells forming the tubules. High mitotic activity was determined in some cases. In the stroma and intertubular areas, a marked coagulation necrosis and mononuclear cell infiltrations consisting of plasma cells and lymphocytes were evident. There were

© 2024 Wiley-VCH GmbH

23656549, 2024, 45, Downloaded from https://chemistry-europe.onlinelibrary.wiley.com/doi/10.1002/slct.202404728 by Erciyes University, Wiley Online Library on [29/11/2024]. See the Terms and Conditions (https://onlinelibrary.wiley.com/terms-and-conditions) on Wiley Online Library for rules of use; OA articles are governed by the applicable Creative Commons License

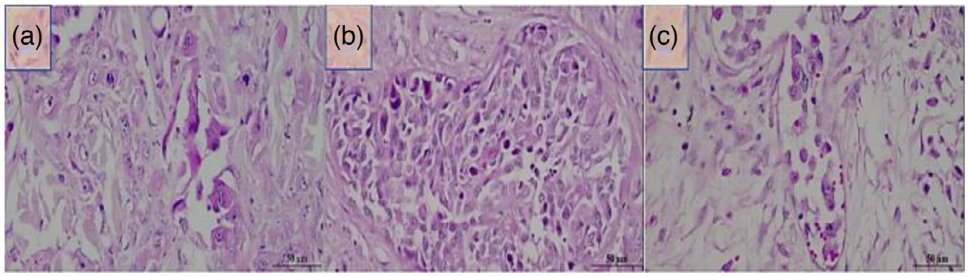


Figure 2. Complex carcinoma of the mammary gland. Staining: Hematoxylin–Eosin. Magnification: 50 µm.

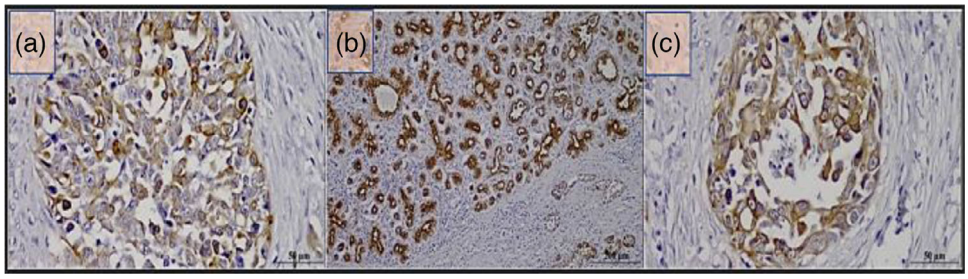


Figure 3. Immunocytochemical characterization of complex carcinoma myoepithelial and luminal cells. (a–c) Pan-cytokeratin (AE1/AE3). ABC method, Gill's hematoxylin counterstain. Magnification: 50 µm.

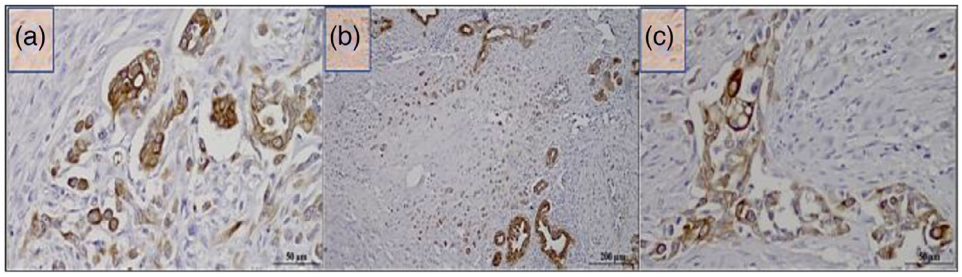


Figure 4. Mammary gland complex carcinoma; dog. Calponin-immunoreactive cells, ABC method, Gill's hematoxylin counterstain. (a, c) Magnification: 50 µm, (b) 200 µm.

areas of increased intercellular mucoid material or embryonal connective tissue (Figure 2a–c).

2.2. Immunohistoapathological Findings

Luminal epithelial cells showed strong expression of cytokeratin AE1-AE3 (Figure 3a–f). Spindle-shaped myoepithelial cells, which participate in the tumor structure and are found in the intertubular areas and stroma, showed strong expression with calponin.

In addition, polygonal shaped hypertrophic myoepithelial cells showed strong expression with calponin (Figure 4a–c).

Spindle-shaped myoepithelial cells showed strong expression with smooth muscle actin (Figure 5a–d).

In all cases of complex carcinoma, moderate expression of vimentin was detected in spindle-shaped myoepithelial cells (Figure 6a–d).

GO has received great attention owing to high surface area with various functional groups on its surface including uncharged polar hydroxyl, epoxide groups, π –bonds and hydrophobic domains. In addition to that it has charged hydrophilic carboxylate groups located at edges. The structure of the vincristine molecule aromatic ring, pi-pi bonds and hydrophobic regions. The vincristine was conjugated on surface of the GO via noncovalent interactions. Although pi-pi stacking interaction in man force to immobilize vincristine on surface on GO, hydrophobic- hydrophobic interaction may provide contribution to make vincristine on GO. 2D and sheet like morphology of GO was seen in Figure 7a.

The surface charges around nanomaterials inducing electrostatic potential is measured by Zeta Potential (ZT) method. Additionally, any modification on nanomaterials causing changes in charge density can be detected by ZT. Although the surface charges of the free vincristine and GO were around −19 mV and −22 mV, respectively as shown in Figure 7b,c, ZT value of Vin@nGO was measured to be around −32 mV (Figure 7d). This increase in ZT measurement may indicate that the vincristine molecule binds to surface of GO to produce Vin@nGO.

Moreover, we exhibited characteristic absorbance peaks of vincristine in free form (Figure 8a) and pristine nGO (Figure 8b) to be ~296 nm and ~230 nm, respectively. After conjugation

© 2024 Wiley-VCH GmbH

23656549, 2024, 45, Downloaded from https://chemistry-europe.onlinelibrary.wiley.com/doi/10.1002/slct.202404728 by Erciyes University, Wiley Online Library on [29/11/2024]. See the Terms and Conditions (https://onlinelibrary.wiley.com/terms-and-conditions) on Wiley Online Library for rules of use; OA articles are governed by the applicable Creative Commons License

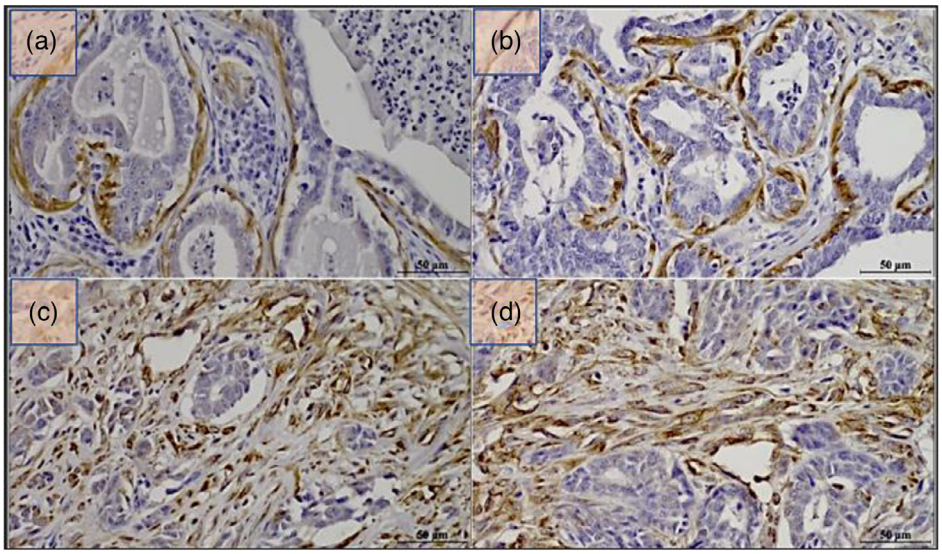


Figure 5. Representative images of α-SMA (α-Smooth muscle actin) expression in the tumor stroma. Tumor stroma fibroblasts positive for α-SMA expression (a–d). ABC method, Gill's hematoxylin counterstain. Magnification: 50 µm.

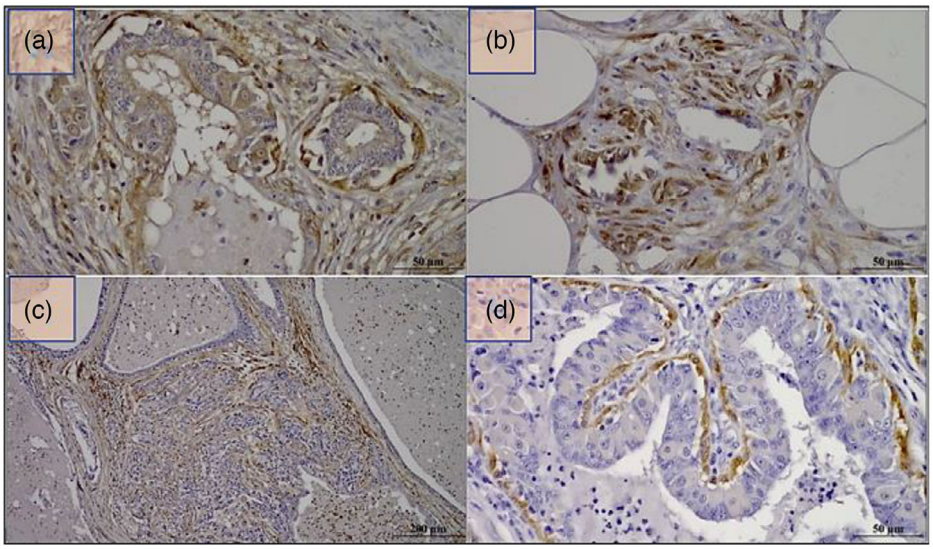


Figure 6. Vimentin immunoreactive cells, ABC method, Gill's hematoxylin counterstain. Magnification: 50 µm (a, b, d), 200 µm (c).

of vincristine on surface of nGO, we displayed both peaks of vincristine and nGO on the same UV-Vis absorbance spectrum (Figure 8c). The loading efficiency of vincristine on surface of nGO for was calculated by following reported work.[42] We drew calibration plot of vincristine for initial loading efficiency on surface of nGO. The plot revealed that as %57 of initial concentration of vincristine was loaded on the nGO.

The reported study showed the highest photothermal efficiency of GO owing to its quite high absorption cross-sections in the NIR region among other NPs used as photothermal agents under the same experimental parameters (concentration, reaction environment, laser wavelength, laser power and time).[10] It can be ideal photothermal agents for hyperthermia treatment in biomedical application.

To determine the concentrations and ideal heat generating capacity of GO, heat generation under NIR laser at different concentrations of GO and Vin@nGO was determined (Figure 9a). The heat generation ability of GO and Vin@nGO under NIR laser irradiation was measured by exposure for 180 sn (3 min) with 20 sn intervals, whereas 10 ppm nGO (blue line) reached around 39 °C in the 60th sn, temperatures of 47 °C and 52 °C were measured in the 120th sn and 180th sn, respectively. When 50 ppm nGO (yellow line) and 100 ppm GO (green line) solutions were exposed to NIR laser, the temperature measurements at 60 sn, 120 sn and 180 sn were 42 °C and 52 °C; 57 °C and 47 °C; 60 °C and 64 °C, respectively.

Each group including i) control cell line (without any treatment), ii) NIR laser irradiation, iii) vincristine, iv) vincristine + NIR laser irradiation, v) GO, vi) GO + NIR laser irradiation, vii) Vin@nGO and viii) Vin@nGO + NIR laser irradiation, was applied to the cells cultured from dog mammary tumor tissue, then each one was incubated for 48 h. After incubation, MTS analysis was

© 2024 Wiley-VCH GmbH

23656549, 2024, 45, Downloaded from https://chemistry-europe.onlinelibrary.wiley.com/doi/10.1002/slct.202404728 by Erciyes University, Wiley Online Library on [29/11/2024]. See the Terms and Conditions (https://onlinelibrary.wiley.com/terms-and-conditions) on Wiley Online Library for rules of use; OA articles are governed by the applicable Creative Commons License

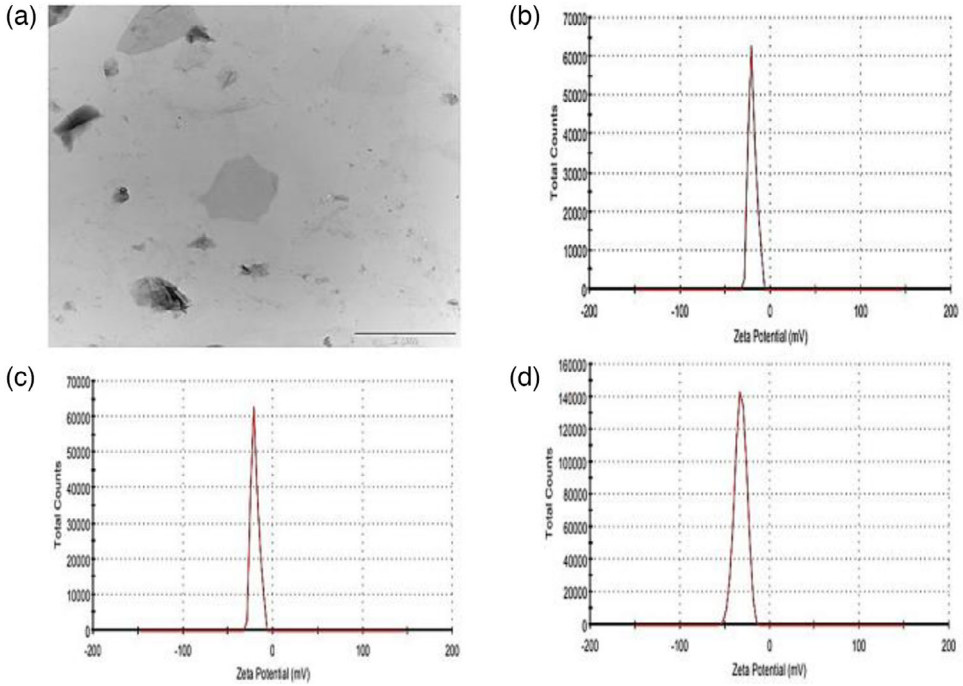


Figure 7. a) TEM image of pristine nGO. Zeta potential values of b) vincristine, c) GO, and d) Vin@nGO.

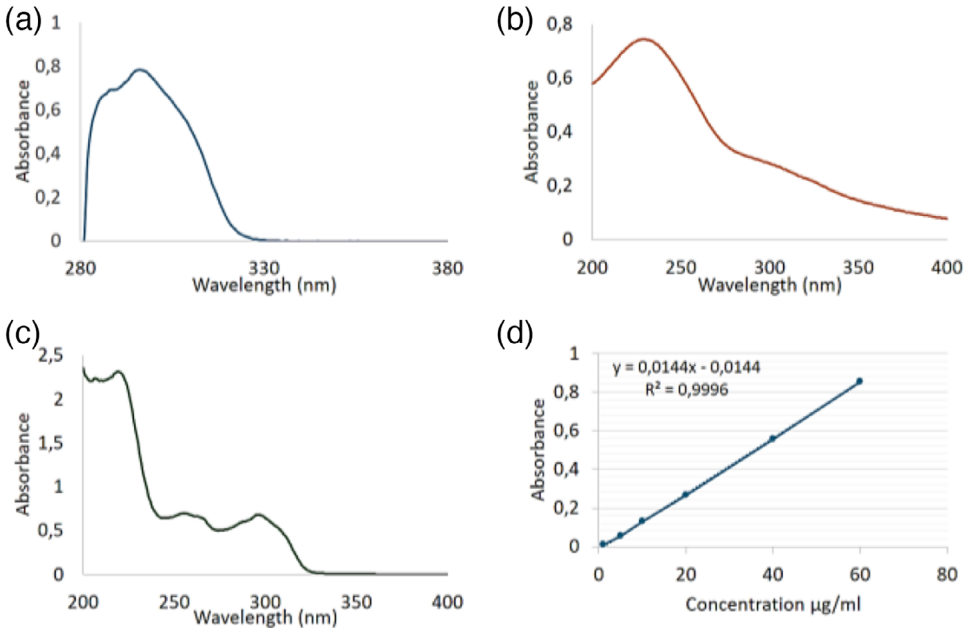


Figure 8. Absorption spectrum of a) Vincristine, b) pristine nGO and c) Vin@GO. d) Calibration plot of vincristine. The loading efficiency of vincristine on nGO was calculated as %57.

performed to test the effect of the treatments applied to the cells on cell viability. According to MTS analysis results, it was found that cell viability decreased significantly after all applications compared to the control group ($p < 0.05$, $p < 0.0001$) (Figure 9b). Compared to the control group, it was found that there was a 40% decrease in the viability of the cells in the NIR-treated groups, a 50% decrease in the cells applied to 25 nM vincristine, and a 60% decrease in the cells to which the combination of NIR and 25 nM vincristine was applied ($p < 0.0001$). In the cells where GO was applied, the cell viability was 25% (($p < 0.05$), in the cells where the GO and NIR combination was applied, it was 40%. However, in the cells where the Vin@nGO combination was applied, it was 50%. As expectedly, when the Vin@nGO was applied to the cell under the NIR laser irradiation, decrease in the cell viability was 90% compared to the control group ($p < 0.0001$). The reason is for effective performance of

© 2024 Wiley-VCH GmbH

23656549, 2024, 45, Downloaded from https://chemistry-europe.onlinelibrary.wiley.com/doi/10.1002/slct.202404728 by Erciyes University, Wiley Online Library on [29/11/2024]. See the Terms and Conditions (https://onlinelibrary.wiley.com/terms-and-conditions) on Wiley Online Library for rules of use; OA articles are governed by the applicable Creative Commons License

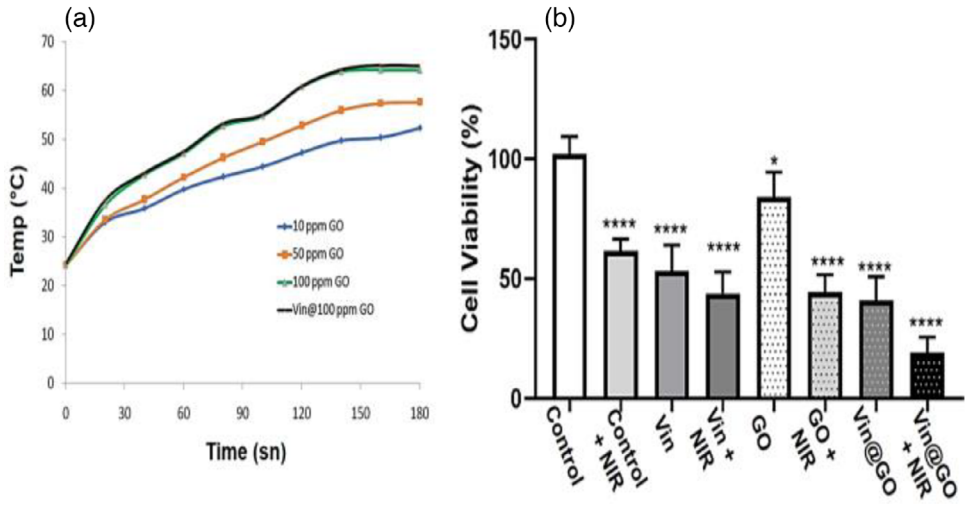


Figure 9. a) Heat generation of 10 ppm GO, 50 ppm GO, 100 ppm GO and Vin@nGO under NIR laser irradiation. b) The cell viability analysis against each applied group.

Vin@nGO in cell destruction is that applying NIR laser irradiation at 808 nm results in heat generation by GO, then target cell become quite vulnerable, then these cells are easily and rapidly killed by chemotherapeutic effect of vincristine instead of free use of GO and vincristine. We demonstrated that the combination of PTT and chemotherapy show quite enhanced killing effect.

3. Conclusion

In report, we prepared Vin@nGO for enhanced PTT and chemotherapies against primary tumor cells obtained from dogs with spontaneous mammary tumors. It is worthy to mention that vincristine knowns as actively used therapeutic agent in clinics conjugated on the surface of GO via pi-pi stacking, however it still showed therapeutic effect as it is in free. Vin@nGO conjugates provided dual and effective therapy for target destruction under the 808 nm NIR laser irradiation. We claim that Vin@nGO and NIR laser with depth penetration property can be used in solid tumor in vivo studies.

4. Experimental Section

4.1. Materials and Methods

4.1.1. Ethical Approval

The study was approved by the Local Animal Ethical Committee (06.11.2019, No.19/212), Kayseri, Turkey. Dogs owner was informed about the study and signed a permission form to use the tumoral tissue removed surgically.

4.1.2. Materials

Vincristine with 2 mg/ 2 mL I.V injection solution (Sterile, cytotoxic) was from Kocak Pharma (Turkey). 3-Aminopropyltriethoxysilane (APTES), $NaNO_3$, H_2SO_4 and $KMnO_4$, Phosphate Buffered Saline (PBS) were obtained from Sigma-Aldrich. Formaldehyde Solution Min % 37 (#104,002.2500) was purchased from Merck. Anti-Vimentin (#ab8069) and Recombinant Anti-Calponin 1 (#ab46794) antiboies were purchased from Abcam. Anti-Cytokeratin AE1/AE3 (#GA05361-2) was purchased from Agilent Technologie. CC/Mount Aqueous Mounting Medium (#C9368) was purchased from Sigma. Penicillin/streptomycin (#PS-B) was purchased from Capricorn Scientific GmbH. Tripsin-EDTA (#03–050–1B), Foetal Bovine Serum (#04–007–1A) and DMEM/F-12 (#01–170–1A) was purchased from Biological Industries. Graphite powder purchased from graphene-supermarket.

4.1.3. Preparation of Tissue Section for the Histopathological Examinations

Tumor tissues were fixed in 10% buffered formalin (pH 7.4) at 4 °C for at least 24 h. Tissue samples were dehydrated through a graded ethanol series (70%, 80%, 90% and absolute) and polished in xylene in a tissue tracking device (Leica TP1020). Next, the tissues were embedded in paraffin and 4 to 5-µm-thick sections were cut on a microtome (Thermo ScientificHM 340E Electronic Rotary Microtome). Two of four sections taken from each blocks were mounted on normal slides and the other two were mounted on adhesive slides for HaematoxylinxEosin. All sections were stained with Haematoxylin-Eosin (HxE) and stained immunohistochemically for cytokeratin AE1/AE3, vimentin, αSMA, calponin antibodies. Streptavidin-biotin peroxidase (SABP) complex method with a commercial kit (Invitrogen, USA) was used for immunohistochemistry and reaction was visualized by aminoethylcarbazole chromogen (AEC, Invitrogen, USA) according to manufacturer's instructions. All slides were photographed using a digital camera (Olympus DP71) attached to a light microscope (BX-51, Olympus) ($\times$ 10, $\times$ 20, $\times$ 40, $\times$ 50) and the images were processed with the DP Controller and DP Manager software.

4.1.4. Animal Source/Source of Mammary Tumor Masses

In this study, tumor tissue was obtained from a 12-year-old, nulliparous, intact female Maltese Terrier breed dog suffering from tumoral masses for 1 year. Tissue samples were collected aseptically during routine surgical treatment procedure at the Education,

© 2024 Wiley-VCH GmbH

23656549, 2024, 45, Downloaded from https://chemistry-europe.onlinelibrary.wiley.com/doi/10.1002/slct.202404728 by Erciyes University, Wiley Online Library on [29/11/2024]. See the Terms and Conditions (https://onlinelibrary.wiley.com/terms-and-conditions) on Wiley Online Library for rules of use; OA articles are governed by the applicable Creative Commons License



Figure 10. Appearance of the tumor mass in the left inguinal mammary lobe (yellow circle) of a terrier dog.

Research and Practice Hospital, Faculty of Veterinary Medicine, Erciyes University. Samples for histopathological and immunohistochemical examinations were preserved in 10% buffered formalin solution. Tissue samples for primary cell culture were placed in microtubes tubes containing medium with penicillin/streptomycin and transferred to the laboratory.

4.1.5. Histochemical Evaluations

For classifying and grading canine mammary tumors, reported system was followed Peña et al. (2013),[39–41] Goldschmidt et al. (2011)[5] and Misdorp et al. (1999).[4] Grading was determined according to the Elston and Ellis scoring system, based on the evaluation of three morphological features: (1) the degree of glandular differentiation assessed by tubular formation; (2) nuclear pleomorphism and (3) mitotic activity. Each parameter was rated with a score of 1–3 according to three categories (1) tubule formation (tumor has more than 75% tubules; <10% tubules; when evaluating tubules, only structures exhibiting lumen will be counted = 3); (2) nuclear pleomorphism (small regular uniform cells = 1, medium nuclear size and variation = 2, and marked nuclear variation = 3) and (3) 10 magnification field fields (HPF; mitotic count for 40 objective lens) second field 0.239 mm^2) (0 to 7 mitoses per 10 HPF = 1, 8–16 mitoses per 10 HPF = 2 and = 17 mitoses per 10 HPF = 3). Scores for all three components were summed to give a total score of 3–9: (1) class I, well-differentiated or low class: 3 5 points; (2) II. Grade, moderately differentiated or moderate: 6–7 points and (3) III. Grade, poorly differentiated or high grade: 8–9 points. Figure 10 show canine mammary tumor before surgical operation.

4.1.6. Histopathological Examinations

Tumor tissues were fixed in 10% buffered formalin solution. Then, the tissue samples were dehydrated in a tissue tracking device (Leica TP1020) containing alcohol and xylene and embedded in paraffin. Breast tissue samples embedded in paraffin. It was cut at a thickness of 5 microns with a microtome (Thermo Scientific HM 340E Electronic Rotary Microtome) and stained with hematoxylin and eosin (HE). Then, the painted sections were examined by digital camera (Olympus DP71) and the program (DP Controller and the DP Manager) under on a compatible light microscope (BX-51, Olympus).

4.1.7. Immuno Histochemical Examinations

The 5 µm thickness tissue samples were placed on slides and coated with 3-aminopropyltriethoxysilane (APTES). Then the sections were deparaffinized and kept in 3% H_2O_2 prepared in methanol for 10 min to eliminate endogenous peroxidase activity. The sections were subjected to heat treatment in citrate buffered solution in a microwave oven (600 watts) for 10 min to remove the masking effect of formalin on the antigenic structure in the tissue and kept in protein blocking serum. After all steps except the protein blocking step, the sections were washed 3 times with phosphate buffer solution (PBS, pH 7.4). The sections were incubated with primary antibodies (cytokeratin AE1/AE3, vimentin, αSMA, calponin) for 1 hr at RT or overnight at + 4 °C, which were then diluted with PBS (pH 7.4). Then, the sections were incubated in biotinized secondary antibody and streptavidin peroxidase for 10 min. Antigenic structures in the tissue became visible under a controlled microscope with AEC chromogen (Zymed Laboratories). Nuclear staining of the sections was done with Mayer's hematoxylin. It was then covered with CC/Mount Aqueous Mounting Medium (Sigma-Aldrich, C9368) and examined under a light microscope (BX-51, Olympus).

4.1.8. Tissue Culture

Tumor tissue incision (1-2 mm) from animals during surgery was placed in microtubes containing medium containing penicillin/streptomycin, then it was immediately placed in trypsin and kept for 1–2 min. The tissue was divided into small pieces in a sterile petri dish and kept in an incubator at 37 °C and 5% CO_2. The medium was added and incubated in an incubator for 7–10 days by renewing every day. The cells were propagated in culture flasks in medium at 37 °C, when the cells reached 70–80% density, the proliferating cells were removed from the surface of the culture flask by using trypsin, and these cells were transferred to sterile tubes. The media was added and centrifuged, then the supernatant was discarded, the pellet remaining at the bottom was mixed with the media, and then it was placed in newly prepared culture flasks. After the first passage, the proliferating cells were frozen in a nitrogen tank at −196 °C until the experiments began. DMSO was used to prevent damage to the cells during the freezing phase, to ensure their continued viability, and to stop intracellular metabolic activity. DMSO was added to the cells dissolved in the medium, and the cells were first stored at −80 °C and then transferred to a liquid nitrogen tank at −196 °C.

4.1.9. Synthesis of Graphene Oxide

The previously reported Hummers and Offeman[44] method was followed. In general, 1 gr exfoliated graphite powder was added into 50 mL H_2SO_4 in an ice bath, then 1 gr $NaNO_3$ and 3 gr $KMnO_4$ were slowly added to the mixture and then it was transferred to a water bath at 36 °C and mixed until it reached the consistency of mud. The temperature was adjusted to 95 °C and heated as an aqueous solution. The black solution turned light brown via hydrogen peroxide (H_2O_2) (30%). The final mixture was centrifuged at 12,000 rpm to obtain GO.

© 2024 Wiley-VCH GmbH

23656549, 2024, 45, Downloaded from https://chemistry-europe.onlinelibrary.wiley.com/doi/10.1002/slct.202404728 by Erciyes University, Wiley Online Library on [29/11/2024]. See the Terms and Conditions (https://onlinelibrary.wiley.com/terms-and-conditions) on Wiley Online Library for rules of use; OA articles are governed by the applicable Creative Commons License

4.1.10. Preparation of Vincristine Conjugated Graphene Oxide (Vin@nGO)

Vincristine (0,2 mg/ 2 mL) solution was mixed with GO aqueous solution (1 mg/mL), then the resulting mixture was incubated overnight under shaking. After incubation, the mixture was centrifuged at 12,000 rpm for 20 min to collect the sample precipitate and to remove the excess or unbound of vincristine via supernatant.[13]

4.1.11. Photothermal and Chemo Therapy

A certain concentration of cancer cell solution ($\sim 10^7$) was mixed with a 100 ppm of Vin@nGO and other materials as shown in other groups. The solution was exposed to light at a wavelength of 808 nm (1.1 W/cm^2) for 5 min. Systematic destruction of cancer cells by photothermal and chemotherapy was examined by MTS assay.

4.1.12. Cell Viability (MTS) Analysis

MTS ((3-(4,5-dimethylthiazol-2-yl)-5-(3-carboxymethocyphenyl)-2-(4-sulfophenyl)-2H-tetrazolium) method was used to detect cell viability. The cancer cell solution ($\sim 10^7$) were prepared into 8 tubes and each tube was incubated with Vin@nGO and other groups (total 8 groups) at RT. Concentration of Vin and GO as 25 nM and 100 ppm, respectively. NIR laser irradiation was applied to 2., 4., 6., and 8. tubes for 5 min. After that, each was transferred to 96-well sterile plates with 1.5×10^3 cells/100 µl medium in each well and incubated in an incubator. 6 repetitions were made for each experiment. Then, the culture was terminated at the 48th h of incubation, and 20 µl of MTS/PMS mixture was added to each box to determine the viability of the cells, and then the absorbance was measured at 450 nm in the ELISA reader. Then, cells in all groups were stained with trypan blue for cell viability and then live cells were counted on the toma slide.

4.1.13. Statistical Analysis

All experiments were repeated 6 times and the obtained data were analyzed using the Graphpad Prism 8.0 program. Student's t test was used in the analyses, and according to the analysis results, results with $p < 0.05$ were considered statistically significant.

Acknowledgments

This work is financially supported by the Erciyes University Scientific Research Office (TSA-2020–9871).

Conflict of Interests

The authors declare no conflict of interest.

Data Availability Statement

The data that support the findings of this study are openly available in [Name] at 10.1002/slct.202404728., reference number 42.

Keywords: Canine mammary tumors · Chemotherapy · Graphene oxide · Photothermal therapy · Vincristine

[1] İ. Kırşan, E. Canoğlu, *Evcil Hayvanlarda Meme Hastalıkları* Vol. *1*, (Eds: M. Kaymaz, M. Fındık, A. Rişvanlı, A. Köker) Medipres, Malatya, **2016**, pp. 317–357.
[2] M. V. R. Kustritz, *Clinical Canine and Feline Reproduction: Evidence-Based Answers*. Wiley Blackwell, Iowa, **2011** pp. 79–122.
[3] A. S. Abdoon, E. A. Al-Ashkar, O. M. Kandil, A. M. Shaban, H. M. Khaled, M. A. El Sayed, M. M. El Shaer, A. H. Shaalan, W. H. Eisa, A. A. G. Eldin, H. A. Hussein, M. R. El Ashkar, M. R. Ali, A. A. Shabaka, *Nanomedicine* **2016**, *12*, 2291–2297.
[4] W. Misdorp, *Histological classification of mammary tumors of the dog and cat.*, Armed Forces Inst. of Pathology, Washington DC, **1999**, *7*, 1–59.
[5] M. Goldschmidt, L. Peña, R. Rasotto, V. Zappulli, *Vet. Pathol.* **2011**, *48*, 117–131.
[6] M. Michishita, *Vet. J.* **2020**, *265*, 105560.
[7] E. Alaçam, *Köpek ve Kedilerde Üreme Süreci ve Sorunları*, Medisan, Vol. *1*, Ankara, **2008**, pp. 127–142.
[8] E. Spyratou, M. Makropoulou, E. P. Efstathopoulos, A. G. Georgakilas, L. Sihver, *Cancers* **2017**, *9*, 1–19.
[9] L. Raduly, R. Cojocneanu-Petric, O. Sarpataki, S. Chira, A. G. Atanasov, C. Braicu, I. Berindan-Neagoe, I. Marcus, *Anim. Sci. Pap. Rep.* **2018**, *36*, 119–148.
[10] I. Ocsoy, N. Işıklan, S. Cansız, N. Özdemir, W. Tan, *RSC Adv.* **2016**, *6*, 30285–30292.
[11] I. Ocsoy, S. Yusufbeyoglu, V. Yılmaz, E. S. McLamoreb, N. Ildız, A. Ülgen, *Colloids Surf. B.* **2017**, *159*, 16–22.
[12] S. Yusufbeyoğlu, V. Cinar, N. Ildiz, Z. Hamurcu, I. Ocsoy, A. Baldemir Kilic, *ChemistrySelect*. **2017**, *9*, e202304893.
[13] B. Tian, C. Wang, S. Zhang, L. Feng, Z. Liu, *ACS Nano* **2011**, *5*, 7000–7009.
[14] C. Li, T. Chen, I. Ocsoy, G. Zhu, E. Yasun, M. You, C. Wu, J. Zheng, E. Song, C. Z. Huang, W. Tan, *Adv. Funct. Mater.* **2014**, *24*, 1772–1780.
[15] J. Wu, Z. Li, Y. Li, A. Pettitt, F. Zhou, *Technol. Cancer Res. Treat.* **2018**, *17*, 1–7.
[16] W. Zhang, J. Dai, G. Zhang, Y. Zhang, S. Li, D. Nie, *Nanoscale Res. Lett.* **2018**, *13*, 379–389.
[17] J. H. Lim, D. E. Kim, E. J. Kim, C. D. Ahrberg, B. G. Chung, *Macromol. Res.* **2018**, *26*, 557–565.
[18] Y. A. Cheon, J. H. Bae, B. G. Chung, *Langmuir* **2016**, *32*, 2731–2736.
[19] R. Lima-Sousa, D. De Melo-Diogoa, C. G. Alvesa, E. C. Costa, P. Ferreira, R. O. Louro, I. J. Correia, *Carbohydr. Polym.* **2018**, *200*, 93–99.
[20] M. A. Ocsoy, S. Yusufbeyoglu, N. Ildiz, A. Ulgen, I. Ocsoy, *ACS Omega*. **2021**, *6*, 20637–20643.
[21] I. Ocsoy, B. Gulbakan, T. Chen, G. Zhu, Z. Chen, M. M. Sari, L. Peng, X. Xiong, X. Fang, W. Tan, *Adv. Mater.* **2013**, *25*, 2319–2325.
[22] N. Temur, S. Dadi, M. Nisari, N. Ucuncuoglu, I. Avan, I. Ocsoy, *Sci. Rep.* **2024**, *14*, 24697.
[23] A. K. Geim, K. S. Novoselov *Nat. Mater.* **2007**, *6*, 183–191.
[24] C. Xu, X. Wang, *Small* **2009**, *5*, 2212–2217.
[25] X. Z. Tang, Z. Cao, H. B. Zhang, J. Liu, Z. Z. Yu, *Chem. Commun.* **2011**, *47*, 3084–3086.
[26] G. Williams, B. Seger, P. V. Kamat, *ACS Nano* **2008**, *2*, 1487–1491.
[27] I. Ocsoy, M. Temiz, C. Celik, B. Altinsoy, V. Yilmaz, F. Duman, *J. Mol. Liq.* **2017**, *227*, 147–152.
[28] S. Arslan, S. Ekrikaya, N. Ildiz, S. Yusufbeyoglu, I. Ocsoy, *Odontology* **2024**, *112*, 341–354.
[29] L. Liu, Q. Ma, J. Cao, Y. Gao, S. Han, Y. Liang, T. Zhang, Y. Song, Y. Sun, *Cancer Nano* **2021**, *12*, 1–31.
[30] A. D. Sontakke, A. Bhattacharjee, R. Fopase, L. M. Pandey, M. K. Purkait, *J. Mater. Sci.* **2022**, *57*, 19019–19049.
[31] L. F. Bulhosa, A. Estrela-Lima, M. da Silva Solcà, G. S. D. Gonçalves, D. F. Larangeira, F. A. de Pinho, S. M. Barrouin-Melo, *Anim. Reprod. Sci.* **2020**, *216*, 106358.
[32] L. R. Raposo, C. Roma-Rodrigues, J. Jesus, L. Martins, A. J. Pombeiro, P. V. Baptista, A. R. Fernandes, *Vet. Comp. Oncol.* **2017**, *15*, 1537–1542.
[33] A. Yamashita, K. Maruo, K. Suzuki, K. Shirota, K. Kobayashi, K. Hioki, *J. Vet. Med. Sci.* **2001**, *63*, 831–836.
[34] R. S. Lewis, J. Fidel, S. Dassanayake, M. H. Court, N. S. Burke, K. L. Mealey, *Vet. Comp. Oncol.* **2017**, *15*, 411–420.

© 2024 Wiley-VCH GmbH

23656549, 2024, 45, Downloaded from https://chemistry-europe.onlinelibrary.wiley.com/doi/10.1002/slct.202404728 by Erciyes University, Wiley Online Library on [29/11/2024]. See the Terms and Conditions (https://onlinelibrary.wiley.com/terms-and-conditions) on Wiley Online Library for rules of use; OA articles are governed by the applicable Creative Commons License

[35] S. Fukumoto, K. Hanazono, T. Komatsu, H. Ueno, T. Kadosawa, H. Iwano, T. Uchide, *Vet. J.* **2013**, *198*, 164–169.
[36] L. F. J. Gaspar, I. Ferreira, M. M. Colodel, C. V. S. Brandão, N. S. Rocha, *Turk. J. Vet. Anim. Sci.* **2010**, *34*, 447–454.
[37] R. Shukla, A. Singh, K. K. Singh, *Drug Deliv. Transl. Res.* **2024**, *14*, 1–16.
[38] J. Škubník, V. S. Pavlíˇcková, T. Ruml, S. Rimpelová, *Biology* **2021**, *10*, 1–25.
[39] L. Peña, P. J. De Andrés, M. Clemente, P. Cuesta, M. D. Pérez-Alenza, *Vet. Path.* **2013**, *50*, 94–105.
[40] W. Misdorp, *Tumors in domestic animals*. 4th ed. Iowa State Press, Ames, USA, **2002**, p. 575.
[41] C. W., Elston, I. O. Ellis, *Assessment of histological grade*, Churchill & Livingstone, London, UK, **1998**, p. 365.
[42] U. Chintapula, S.-U.l Karim, P. R. Iyer, H. Asokan-Sheeja, B. Neupane, F. Nazneen, H. Dong, F. Bai, K. T. Nguyen, *Nanoscale Adv.* **2024**, *6*, 3747–3758.
[43] O.I.A. Savchuk, J. J. Carvajal, J. Massons, M. Aguilo, F. Díaz, *Carbon* **2016**, *103*, 134–141.
[44] W. S. Hummers Jr., R. E. Offeman, *J. Am. Chem. Soc.* **1958**, *80*, 1339.

Manuscript received: October 04, 2024

© 2024 Wiley-VCH GmbH

23656549, 2024, 45, Downloaded from https://chemistry-europe.onlinelibrary.wiley.com/doi/10.1002/slct.202404728 by Eotvos University, Wiley Online Library on [29/11/2024]. See the Terms and Conditions (https://onlinelibrary.wiley.com/terms-and-conditions) on Wiley Online Library for rules of use; OA articles are governed by the applicable Creative Commons License